Power Electronics and Drives
Volume 11(46), 2026 DOI: 10.2478/pead-2026-0005

Power Electronics and Drives

Experimental Evaluation of Current Sensors' Fault Detection and Classification Methods in PMSM Drives

Research Paper

Kamila Anna Jankowska*

Department of Electrical Machines, Drives and Measurements, Wroclaw University of Science and Technology, Wrocław, Poland

Received: 03 December, 2025; Received in the revised form: 12 February, 2026; Accepted: 19 February 2026

Abstract: This study presents a comparative analysis of fault detection and classification systems developed for current sensors in a drive system with a permanent magnet synchronous motor (PMSM). The research focuses on a fault detection algorithm based on current signal markers and on classification systems employing both shallow and deep neural network architectures. The study aims to evaluate the effectiveness, accuracy, and robustness of these methods in identifying sensor faults that may influence the performance and stability of the drive control system. Experimental verification was carried out using the same Moog 0.894 kW motor, tested under various load and speed conditions to ensure reliable comparison and validation of the obtained results.

Keywords: *current-sensor faults • neural classifier • fault-tolerant control • CNN • MLP*

1. Introduction

The current-sensor faults in electric-motor–drive systems represent a rapidly developing area of research (Li et al., 2019; Nesri et al., 2024; Zhu et al., 2024). These sensors play a crucial role in the electric drive control system. Consequently, any malfunction or inaccuracy in current sensing can have a significant impact on the performance and reliability of the entire drive system. Such faults can lead to serious, and in some cases even catastrophic, consequences. Depending on the type of failure, the control system may lose stability, and its operational performance can deteriorate (Khil et al., 2017). Therefore, the detection, isolation, and compensation of current-sensor faults have become essential aspects of modern fault-tolerant control strategies for electric drives (Zhang et al., 2025).

In electric drive systems, current transducer manufacturer (LEM)-type current transducers are commonly used. These sensors provide non-invasive current measurement. In the literature, several basic types of faults are usually considered (Zhang et al., 2018, 2025):

- complete or intermittent loss of the measurement signal due to damaged electronic components or wiring,
- gain errors, measurement noise, and offset caused by the degradation of magnetic properties or corrosion of the core resulting from temperature changes.

In the available literature, several groups of methods can be distinguished for the detection, classification, and compensation of measurement sensors' faults. In the case of current sensors, signal-based approaches are the most commonly used (Khojet et al., 2019; Zhao et al., 2025). These methods are among the simplest and mainly

* Email: kamila.jankowska@pwr.edu.pl

applied for fault detection and identification of the faulty phase. Fault information is obtained through operations performed on the current signals (Khil et al., 2019) and, in some cases, also from measurements provided by the speed transducer (Guo et al., 2021). In recent studies, it has become clear that within research relying on signal-analysis methods, the primary emphasis has shifted beyond merely detecting and locating faulty sensors towards the classification of the specific type of damage (Li et al., 2025; Zhang et al., 2025; Zheng et al., 2025). In such studies, the authors seek additional indicators characteristic of particular types of faults, such as the gain factor and the offset coefficient. This approach requires detailed preliminary analysis and advanced *a priori* knowledge, which can be a drawback due to the additional complexity and expertise needed. An example can be an article (Li et al., 2025) where the authors present a harmonic-current–based method for diagnosing current-sensor faults in dual three-phase permanent magnet synchronous motors (PMSMs) for electric aircraft. The technique exploits the relationship between harmonic (*x*–*y*) and zero-sequence (o_1–o_2) currents under faults, using second-order differencing and adaptive thresholds to quickly and reliably detect subtle deviations.

Recently, there has been a growing number of studies employing model-based methods (Haghgooei et al., 2023; Jawdeh et al., 2025; Xiaobing and Shangbo, 2022; Zhang et al., 2025). In such approaches, various types of state variable estimators are used. A significant advantage of these fault detection and localisation methods is the possibility of simultaneous fault compensation. In their article Xiaobing and Shangbo (2022) focus on fault diagnosis and fault-tolerant control for PMSM systems using observers. They employ algebraic differential observation combined with a current linear extended state observer (LESO) and space vector error projection to estimate faulty phase currents. Another example is the article by Haghgooei et al. (2023), where the authors use observers to detect current-sensor faults in the wound rotor synchronous machine (WRSM). A flux-based observer estimates stator currents and triggers a switch to sensorless control when a fault occurs. Analysing recent studies in the literature on model-based methods, authors often utilise sliding mode observers (SMOs). An example of such work is the study by Zhao et al. (2017), which proposes a scheme for reconstructing current-sensor faults and estimating unknown load disturbances in a PMSM-driven system. The method employs two SMOs to handle load disturbances and sensor faults separately. Xu et al. (2024) proposed a method for detecting incipient faults in PMSM current sensors using an adaptive interval SMO. The approach reconstructs sensor faults and estimates the state accurately, enabling diagnosis of both incipient and severe faults. Another example of such work is the article by Tarkhani et al. (2025), which presents a fault-tolerant control scheme for a three-phase induction motor under current-sensor failure conditions, combining a third-order super-twisting sliding mode controller with a third-order super-twisting SMO. Speed sensor fault detection and compensation can also be effectively achieved using SMO-based techniques (Jankowska et al., 2023). The above literature review highlights the complexity of applying model-based methods for fault detection in PMSM systems, which often involves combining multiple approaches. In studies presenting model-based methods, there is also an effort to utilise additional indicators that enable fault classification (Haghgooei et al., 2023; Jawdeh et al., 2025).

Currently, there is an increasing number of studies on signal- and model-based methods. Signal-based approaches often face challenges in accurately classifying faults, while model-based methods require detailed *a priori* knowledge. Moreover, in such studies, authors typically do not provide extensive statistical analysis across different operating conditions; instead, they base their conclusions on individual signal traces. Furthermore, it is worth highlighting that model-based methods are more challenging to implement in PMSMs than in induction motors due to strong non-linearities and sensitivity to parameter variations (Li et al., 2025; Sergakis et al., 2025). Consequently, hybrid approaches combining observers with machine learning or signal-based techniques are often employed to enhance fault detection and identification in PMSMs (Chen et al., 2025).

The last category of methods – those based on artificial intelligence, mainly neural networks – has been the least covered in the literature. In this case, the focus is not merely on fault detection or localisation but primarily on fault classification. For fault-type classification, neural networks – most commonly with feedforward architectures – are the most widely used (Jankowska and Dybkowski, 2023; Teler et al., 2024). There are also examples of more complex network structures, such as convolutional neural networks (CNNs) and long short-term memory networks (LSTMs), which allow for more effective identification of different fault types (Wu et al., 2024; Teler et al., 2024). A slightly different application of LSTM is presented in a study (Wang et al., 2025), where a current-sensorless fault-tolerant control strategy for PMSMs is proposed to improve the reliability of electric propulsion in electric aircraft. The approach combines hierarchical fault diagnosis using a SMO with LSTM-based current reconstruction, enabling direct mapping from speed/position to phase currents during sensor failures. Another example (Chen et al., 2025) proposed a fault detection and identification method for PMSM current sensors by integrating an attention mechanism

with a bidirectional LSTM (BiLSTM) network to capture temporal dependencies in the signals. These methods have been applied before to classify other types of faults, and as a result, much of the current-sensor faults research builds on the insights gained from those earlier applications (Baharvand et al., 2024; Li et al., 2022; Ma et al., 2025; Yan and Sun, 2023). It is worth noting that the authors of the studies using this approach typically present results from both simulation and experimental analyses across a wide range of drive system operating conditions. The main drawbacks of neural network–based methods are their computational complexity and the time required for fault detection and classification.

In this study, a comparative analysis of various methods for monitoring current-sensor condition in a PMSM drive system is presented. The investigation focuses on the use of current markers (Cri) for fault detection and localisation, as well as on the application of both shallow and deep neural networks for fault classification. The authors focus on analysing methods that do not require knowledge of the motor model because such approaches are generally more robust to parameter variations and easier to implement in practical applications, particularly in PMSMs. The analysis is based exclusively on experimental data from the same motor, with the performance of the algorithms evaluated under a wide range of operating conditions to assess reliability, accuracy, and robustness. This study stands out because it offers a broad comparative evaluation of various approaches based on parameters such as classification accuracy, effectiveness, and computational complexity, rather than focusing on individual methods separately. The main contributions of the paper are as follows:

- presenting a comprehensive cross-sectional overview of fault diagnosis possibilities for current sensors using methods that do not require knowledge of the motor model, in contrast to most existing studies, which typically focus on a single method; this paper compares and evaluates several model-free methods applied to the same motor and control structure,
- analysis of selected diagnostic methods in terms of their effectiveness, supported by statistical analysis, as well as their computational complexity under variable operating conditions,
- proposal of an improvement of an existing diagnostic approach based on Cri markers, aimed at increasing the efficiency and robustness of the damaged phase localisation.

The rest of this paper is organised as follows. The second section is a description of the experimental set-up, the analysed failures, and the method of their simulation in the control system. Sections 3–5 present the characteristics of the individual fault detection and classification systems, as well as an evaluation of their effectiveness. The last section provides a summary of the work along with a comparative analysis of all the methods.

2. Experimental Set-Up and Fault Analysis

The experiments were carried out on a PMSM with a rated power of 0.894 kW, whose basic parameters are presented in Table 1. As a load for the tested motor, a second Moog motor with a torque of 1.4 Nm was used, controlled by a dedicated Moog MSD servo-drive (East Aurora, NY, USA).

The field-oriented control (FOC) structure was developed in the MATLAB/Simulink (MathWorks, Natick, MA, USA) environment and implemented on a dSPACE 1103 (Paderborn, Germany) control board. The motor was supplied by a Pulse Width Modulation (PWM)-controlled inverter operating at a switching frequency of 15 kHz.

Feedback signals in the control structure were obtained using an incremental encoder (36,000 pulses per revolution) and LEM-type (LA 25-P) current transducers. The sampling period was the same for both the current and the speed feedback signals and was set to 1×10^{-4} s. The current was measured in all three phases; however, in the control structure, only the measurements from phases A and B were used to determine the stator current components. The current in phase C was measured solely for diagnostic purposes and utilised in the Cri-based detection scheme as well as in the classifier based on shallow neural networks. A block diagram and photos of the individual components of the test stand are shown in Figure 1.

Table 1. Essential parameters of the tested motor.

P_N (kW)	P_p (–)	n_N (rpm)	T_N (Nm)	I_N (A)	J (kg . m^2)	R_s (Ω)	L_s (mH)
0.894	4	6,200	1.4	1.9	0.000039	4.6615	7.9835

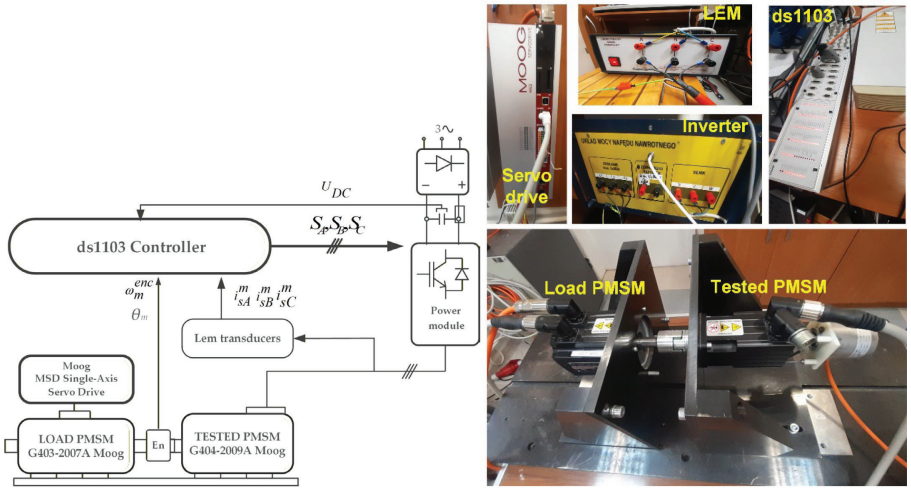

(a) (b)

Figure 1. Block diagram (a) and photos (b) of experimental set-up. PMSM, permanent magnet synchronous motor.

In this set-up, faults were simulated using equations that describe gain error, measurement noise, and signal loss (Table 2). The fault simulation consisted of introducing modifications to the measured signal, which were then used in the control structure. As a result, the effect of the fault became visible within the control system, influencing its operation and allowing for analysis of the diagnostic algorithms. A block diagram of the control system, showing the measurement systems and the signals used for fault detection and classification, is presented in Figure 2.

Table 2. Types of individual failures and equations that enable their simulation.

Type of the fault	Current value
Gain error	$i_A^{fault} = (1-\gamma) i_A^{meas}$
Signal noise	$i_A^{fault} = i_A^{meas} + n(t)$
Signal loss	$i_A^{fault} = 0$

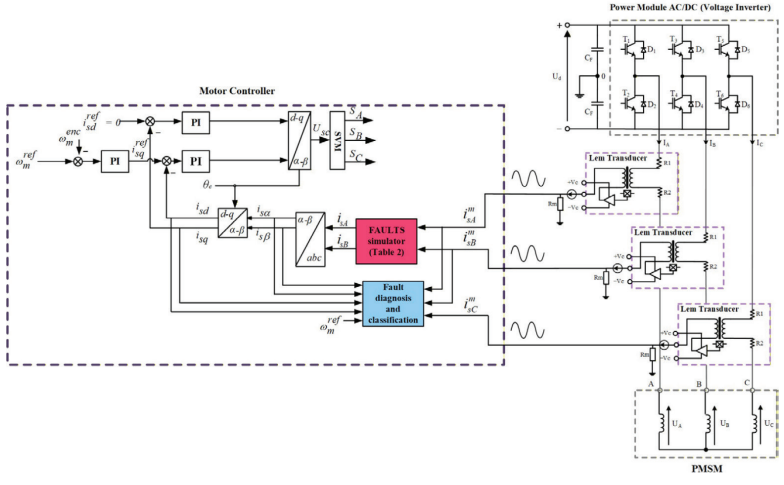

Figure 2. Control system diagram with measurement systems. PMSM, permanent magnet synchronous motor.

Figure 3 shows example waveforms for the analysed faults in phase A. The article analyses signal loss, signal noise with added to measurement white Gaussian noise at a level of 70 dB, and gain error with a value of $0.9i_A^{meas}$.

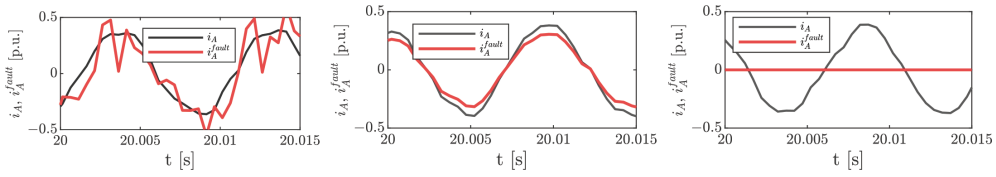

(a) (b) (c)

Figure 3. Sample transients with different types of faults – signal noise (a), gain error (b), and signal loss (c).

3. Fault Detection Based on Cri Markers

The first method to be described is fault detection using current markers Cri (Bahri et al., 2007; Klimkowski and Dybkowski, 2015; Jankowska and Dybkowski, 2022). This method is based on the fact that the currents in the *α-β* coordinates can be determined using measurements from two or three current sensors in the following way:

$$i_{s\alpha 1} = \frac{2}{3}(i_{sA} - \frac{1}{2}(i_{sB} + i_{sC})), i_{s\beta 1} = \frac{\sqrt{3}}{3}(i_{sB} - i_{sC}) \tag{1}$$

$$i_{s\alpha 2} = i_{sA}, i_{s\beta 2} = \frac{\sqrt{3}}{3}(i_{sA} + 2i_{sB}) \tag{2}$$

$$i_{s\alpha 3} = -(i_{sB} + i_{sC}), i_{s\beta 3} = -\frac{\sqrt{3}}{3}(i_{sB} - i_{sC}) \tag{3}$$

In each case, these values should be equal or, under real conditions, differ only slightly. Based on this, a condition (Δ) can be established which, if violated, indicates the presence of a fault in one of the sensors:

$$(i_{s\alpha 1} = i_{s\alpha 2} = i_{s\alpha 3}) \wedge (i_{s\beta 1} = i_{s\beta 2} = i_{s\beta 3}) \tag{4}$$

Since the previous condition allows only the detection of a fault in one of the three sensors, it is necessary to introduce additional conditions that enable the localisation of the faulty phase. Eqs (1)–(3) make it possible to determine three current markers, each independent of one phase measurement:

$$C_{ri1} = (-(i_{sB} + i_{sC}))^2 + (\frac{\sqrt{3}}{3}(i_{sB} - i_{sC}))^2 \tag{5}$$

$$C_{ri2} = (i_{sA})^2 + (-\frac{\sqrt{3}}{3}(i_{sA} + 2i_{sC}))^2 \tag{6}$$

$$C_{ri3} = (i_{sA})^2 + (\frac{\sqrt{3}}{3}(i_{sA} + 2i_{sB}))^2 \tag{7}$$

The relationships between the markers after a fault occurs make it possible to locate the fault. Since the differences between the markers from the current and previous samples have a significant impact on improving detection stability, they were included in the algorithm in the following way:

$$\Delta C_{rij} = |C_{rij}(k) - C_{rij}(k-1)| \text{ for } j = 1,2,3 \tag{8}$$

In the standard version of the algorithm, the localisation of the faulty phase is performed using the relationships between the current markers, applied in the following way $C_{ri1} < C_{ri3} < C_{ri2}$ for phases A and B. In this work, the author modified the algorithm, showing that it is sufficient for the independent marker to have the smallest value among all markers to locate the damage (Figure 4). This modification was introduced to improve the effectiveness and robustness of the fault localisation, while maintaining the fundamental principles of the original method.

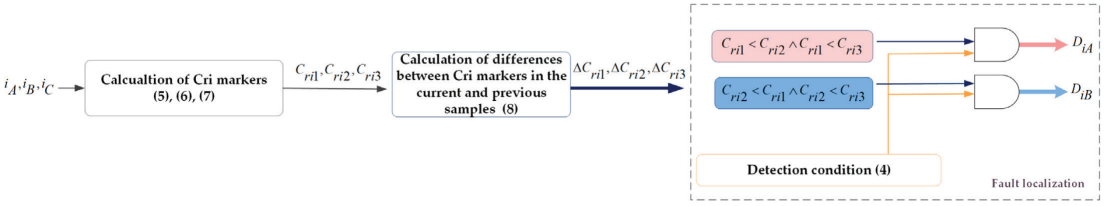

Figure 4. Block diagram of the phase detection and localisation system based on Cri markers.

To demonstrate the significance of the proposed enhancement, Figures 5 and 6 illustrate the detector performance under fast periodic signal interruptions. As shown in Figure 5, the standard version of the detection algorithm exhibits a higher number of phase localisation errors, whereas the improved algorithm presented in Figure 6 significantly reduces these misclassifications. The improvement in detection accuracy is particularly noticeable in phase A.

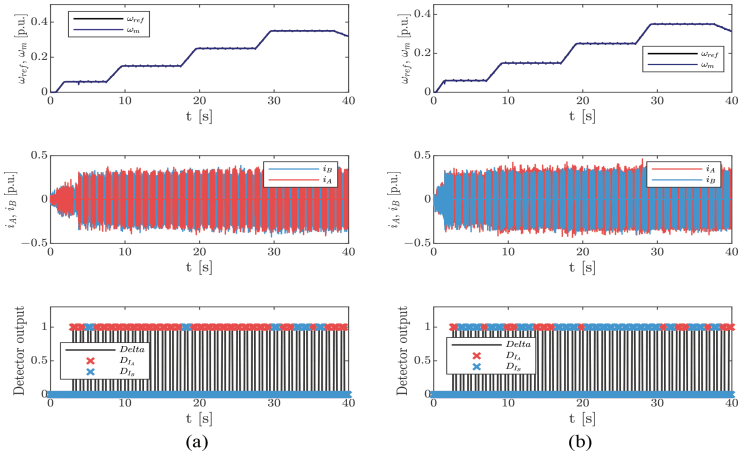

Figure 5. Speed, current, and detector response waveforms in the standard version during periodic signal interruption in phases A (a) and B (b).

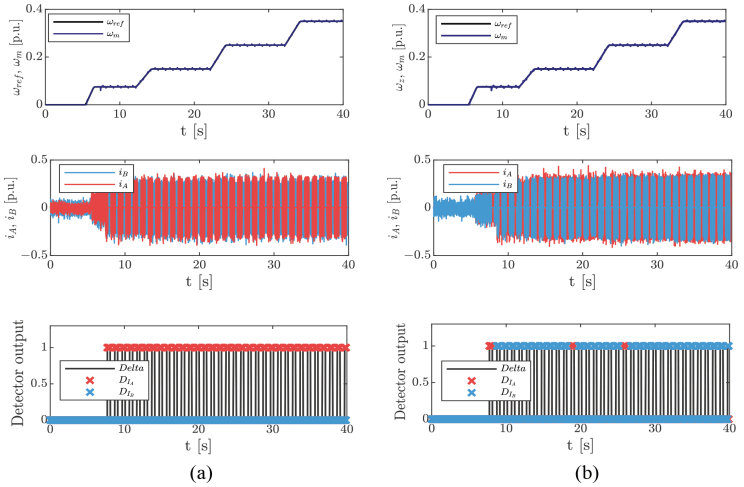

Figure 6. Speed, current, and detector response waveforms in the modified version during periodic signal interruption in phases A (a) and B (b).

With the use of the modified version of the algorithm, example results of fault detection and localisation in phases A and B for a loaded motor during measurement signal loss are presented in Figure 7. These results indicate that, from the detection perspective, the difference between the marker values in the current and the previous samples – caused by the occurrence of the fault – is more significant than the absolute instantaneous values of the individual markers.

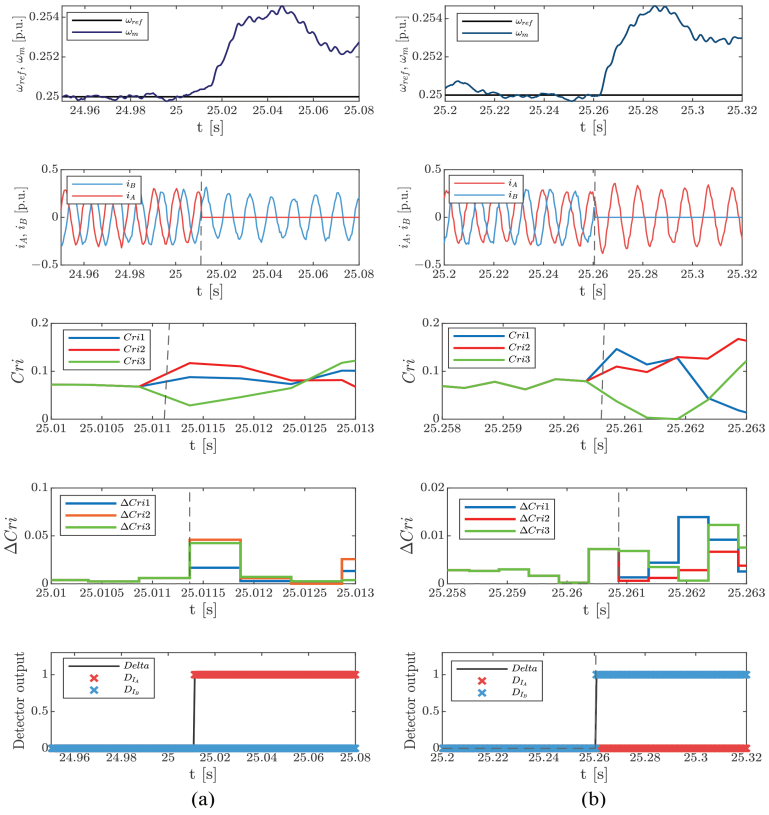

Figure 7. Waveforms of speed, current, markers, marker differences, and detector response during signal loss in phases A (a) and B (b).

As another example, a fault with a significantly smaller impact on the control structure is presented—measurement noise in phases A and B (Figure 8). In this case, the differences between the marker values before and after the fault occurrence are much smaller; however, the fault is still correctly detected and located.

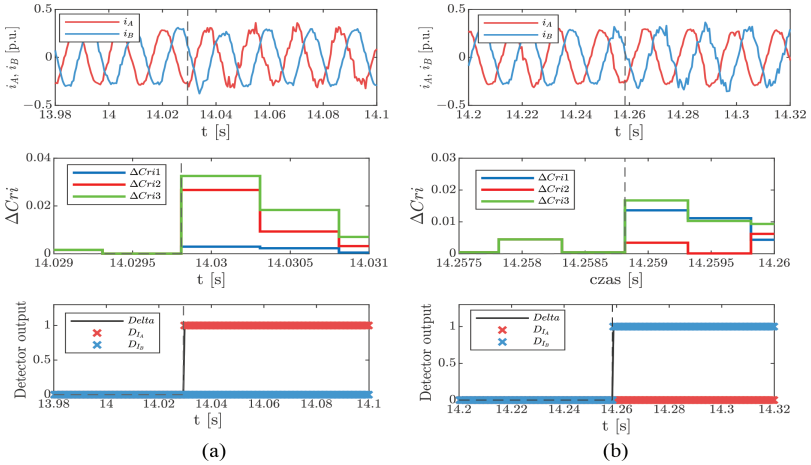

Figure 8. Waveforms of speed, current, markers, marker differences, and detector response during signal noise in phases A (a) and B (b).

The final verification of the system's effectiveness was carried out for several speed values under a loaded motor condition (0.15 T_N) and for all considered types of faults. The results were presented in the form of a truth matrix (Figure 9), allowing for a precise assessment of the system's performance and the identification of any potential malfunctions. The results also take into account the number of tested samples. Based on the obtained results, the small differences observed in fault detection between phases A and B can be explained by the slightly greater influence of phase A on the control structure, as it contributes to the calculation of both current components in the stator *α–β* reference frame and by the slightly different number of samples used in the experiments

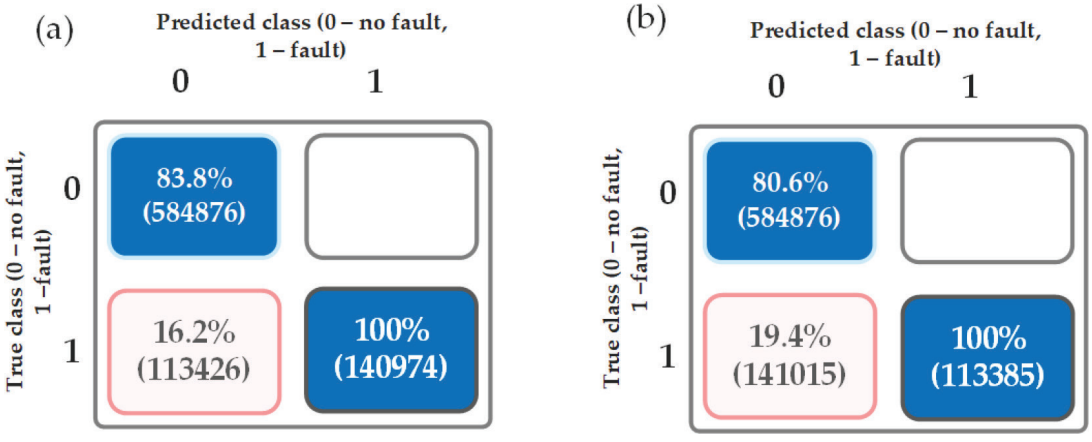

Figure 9. Confusion matrices for the detector based on Cri markers for phases A (a) and B (b).

4. Fault Classification Based on MLP

The next method presented is a neuralfault classifier based on a feedforward multilayer perceptron (MLP) network. The experiments were conducted using a network with two hidden layers (33 and 10 neurons). The number of neurons in the first hidden layer depended on the number of network inputs (N), according to the rule (2N + 1) (Bishop, 1996).

The input data to the network consisted of current signals – present values and previous samples in phases A and B, currents in the rotor reference frame (*d–q*), the modulus of the space vector, and the speed. The classification system also included the Delta $(\Delta i_{s\alpha\beta})$ signal from the previous algorithm, which indicates the occurrence of a fault but does not provide its location. Therefore, the task of the network is solely the localisation and classification of the fault. The $\Delta i_s\alpha\beta$ signal is used as an essential input for the MLP classifier. Thanks to this signal, the network only needs to perform fault classification, which significantly improves its accuracy. The complete input vector had the following form:

$$\begin{aligned}&[i_{sA}(k),\ i_{sA}(k-1), i_{sA}(k-3),\ i_{sA}(k-5),\ i_{sA}(k-7),\\ &i_{sB}(k),\ i_{sB}(k-1),\ i_{sB}(k-3),\ i_{sB}(k-5),\ i_{sB}(k-7),\\ &\omega_{ref},\ \ \Delta i_{s\alpha B},\ \ |I_S|,\ \ \ i_{sd},\ \ \ i_{sq},]^T\end{aligned} \tag{9}$$

The training and test data were prepared based on several different values of the set speed and motor load. The parameters of the training and testing data are presented in Table 3.

The network output was a two-dimensional vector – corresponding to each of the two analysed phases – and, depending on the type of detected fault, indicated the following: 0 – no fault, 1 – signal loss, 2 – measurement noise.

As the main element of verification of the analysed classifier, confusion matrixes for the test data, according to Table 3, were presented separately for the outputs corresponding to phases A (Figure 10a) and B (Figure 10b). The data are shown both as absolute values (the number of correct and incorrect classifications) and in percentage

Table 3. Parameters of training and testing data for the classifier based on MLP.

Feature	Training data	Testing data
Number of samples	380,010	228,006
Speed	$\pm 0.1\omega_{ref}$, $\pm 0.2\omega_{ref}$, $\pm 0.3\omega_{ref}$	$\pm 0.075\omega_{ref}$, $\pm 0.15\omega_{ref}$, $\pm 0.225\omega_{ref}$
Motor load	0.1 T_N, 0.3 T_N	0.2 T_N
Regenerative mode	0.1 T_N, 0.3 T_N	0.2 T_N

MLP, multilayer perceptron.

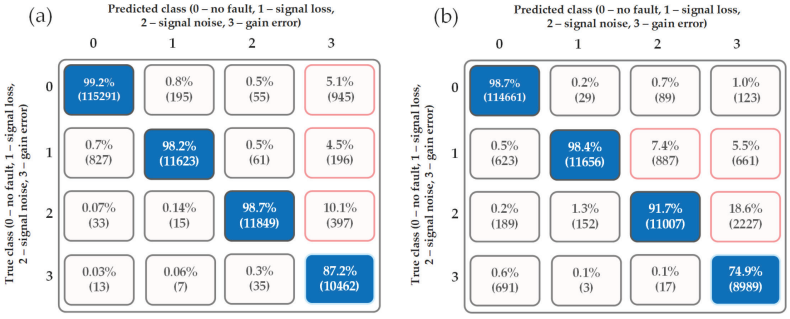

Figure 10. Confusion matrices for the classifier based on MLP for phases A (a) and B (b) for the test data. MLP, multilayer perceptron.

form, which allows for an easier assessment of effectiveness regardless of the data size. The classifier showed the greatest difficulties in the case of gain error, which proved to be the most challenging to identify correctly, particularly for phase B.

In addition to the detailed effectiveness results for individual outputs, example online classification transients are also presented after implementing the neural classifier on the experimental set-up. The online tests were carried out under operating conditions consistent with the test data, for both the unloaded and the loaded motor. The waveforms illustrate the classifier's operation during signal loss and measurement noise occurrences in phases A (Figure 11a) and B (Figure 11b). Based on the classifier output waveforms, the fault location and type can be clearly identified. Additionally, slightly higher effectiveness was observed for the loaded motor.

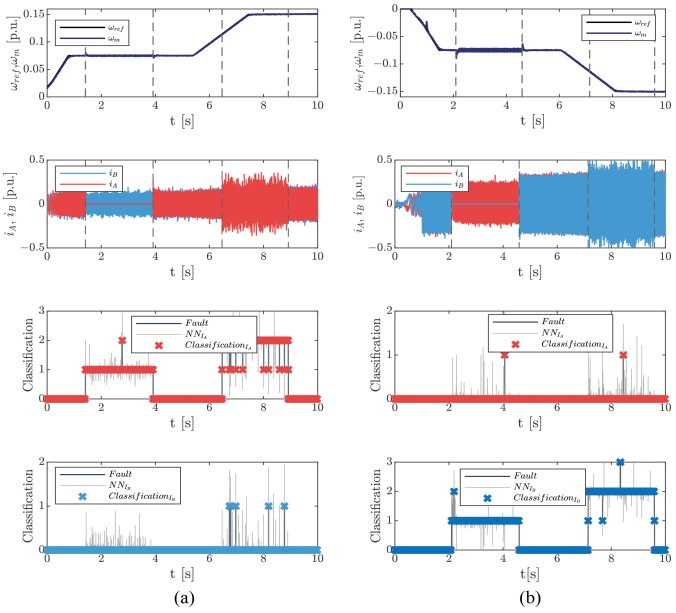

Figure 11. Speed, current, and classifier outputs transients during signal loss and signal noise for no-load conditions in phase A (a) and loaded motor conditions in phase B (b).

Table 4. Parameters of training and testing data for the classifier based on CNN.

Feature	Training data	Testing data
Number of samples	69,800	69,800
Number of training examples	698	698
Speed	$\pm 0.05\omega_{ref}$, $\pm 0.1\omega_{ref}$, $\pm 0.2\omega_{ref}$ $\pm 0.3\omega_{ref}$	$\pm 0.07\omega_{ref}$, $\pm 0.15\omega_{ref}$, $\pm 0.25\omega_{ref}$ $\pm 0.35\omega_{ref}$
Motor load	0.1 T_N, 0.2 T_N	0.15 T_N, 0.25 T_N
Regenerative mode	0.1 T_N	0.15 T_N

CNN, convolutional neural network.

The following examples present faults for the unloaded system in phase B. As shown in Figure 12a, the absence of load also reduces the classifier's effectiveness. The performance decreases further as the rotational speed increases. The final example (Figure 12b) illustrates faults that exert a comparatively smaller influence on the control structure for the unloaded drive system in phase B. In this case, the classifier exhibits errors only between these specific fault types, indicating that their characteristics are highly similar and therefore more difficult to distinguish.

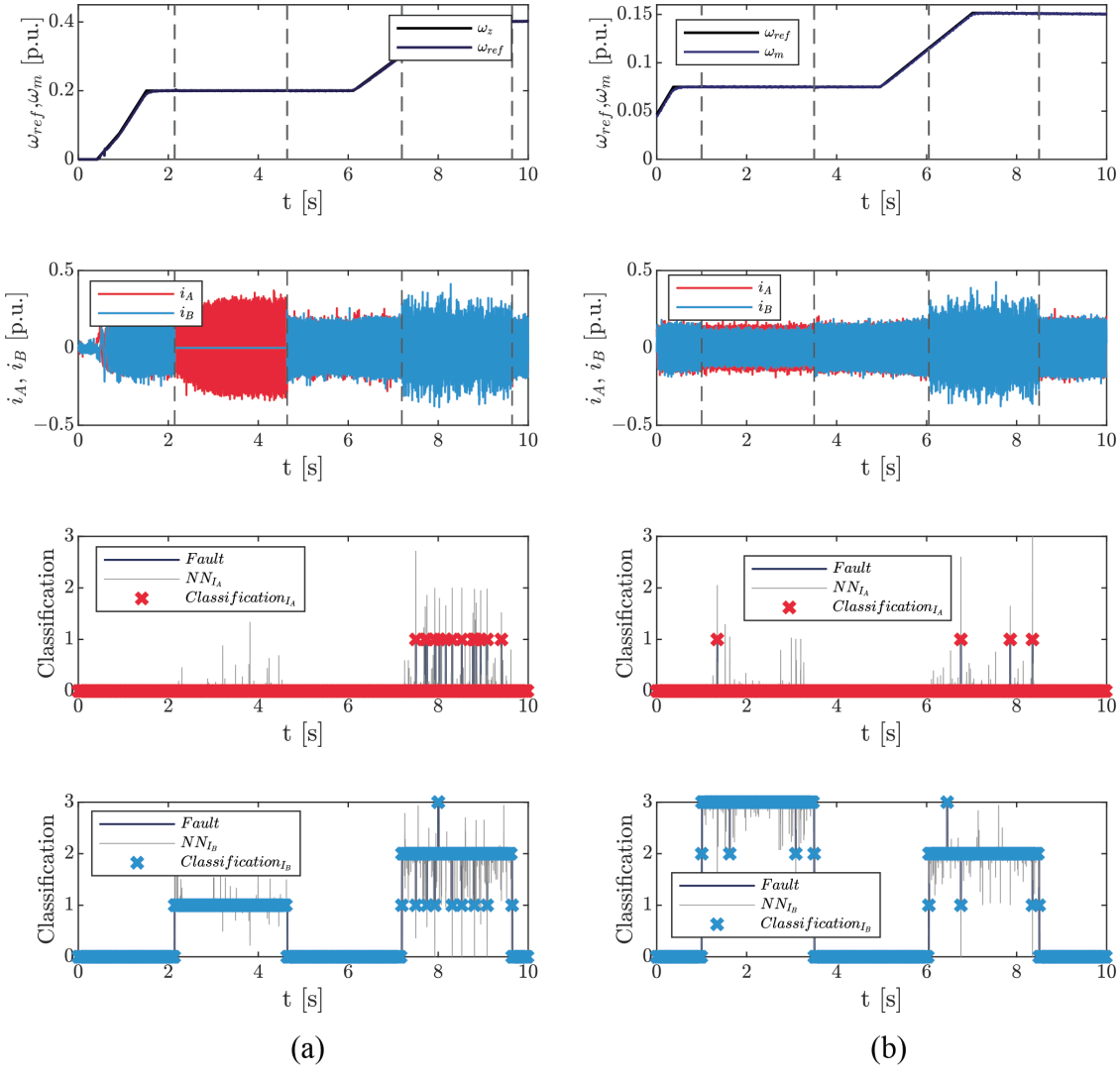

Figure 12. Speed, current, and classifier outputs transients during faults in phase B.

5. Fault Classification Based on CNN

Another classifier was developed based on CNN. In comparison with the previously presented shallow network solution, the key difference lies not only in the network architecture but also in the characteristics of the input data. The network input is a 40 × 10 matrix composed of four 10 × 10 signals: the phase currents *isA* and *isB*, and the *iq* and *id* components in the rotor reference frame. For this reason, different training and testing data with the parameters shown in Table 4 were used.

For classification, two independent neural networks with identical structures were employed, operating in parallel, which enables independent analysis of each phase. The output of each network takes a value in the range of 1–4 (the output is shifted by one with respect to the classifier based on the MLP), corresponding to one of the four analysed fault classes. The detailed structure of the neural network is presented in Table 5. Its design is based on solutions available in the literature (Yan and Sun, 2023; Skowron et al., 2022), taking into account proven configurations used in classification tasks. Additionally, the principle of gradually increasing the network depth was applied, starting with 90 filters in the first convolutional layer and ending with 180 filters in the fourth layer.

Table 5. Structure of the CNN classifier network.

Input layer: Matrix 40 × 10			
Feature detector			
Convolutional layer 3 × 90 Padding method: same	Batch normalisation layer	Activation function: ReLu	MaxPooling layer Stride: 20
Convolutional layer 3 × 120 Padding method: same	Batch normalisation layer	Activation function: ReLu	MaxPooling layer Stride: 2
Convolutional layer 3 × 150 Padding method: same	Batch normalisation layer	Activation function: ReLu	MaxPooling layer Stride: 2
Convolutional layer 3 × 180 Padding method: same	Batch normalisation layer	Activation function: ReLu	MaxPooling layer Stride: 2
Classification			
Fully connected layer (4)	Softmax layer	Classification layer	
Output layer: 1 – no fault, 2 – signal loss, 3 – signal noise, 4 – gain error			

CNN, convolutional neural network.

In this case, the confusion matrices are also presented first (Figure 13). The achieved effectiveness, particularly in the case of gain error, is at a significantly higher level with respect to the classifier based on the MLP.

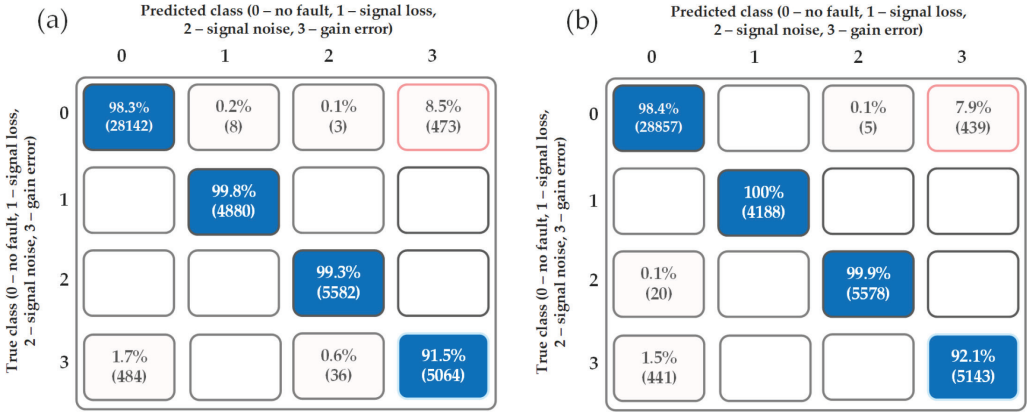

Figure 13. Confusion matrices for the classifier based on CNN for phases A (a) and B (b) for the test data.

The further verification of the classifier's performance is based on example waveforms during a signal loss in phases A (Figure 14a) and B (Figure 14b). The waveforms are consistent with the classification matrices, confirming a lower number of incorrect responses in the CNN structures.

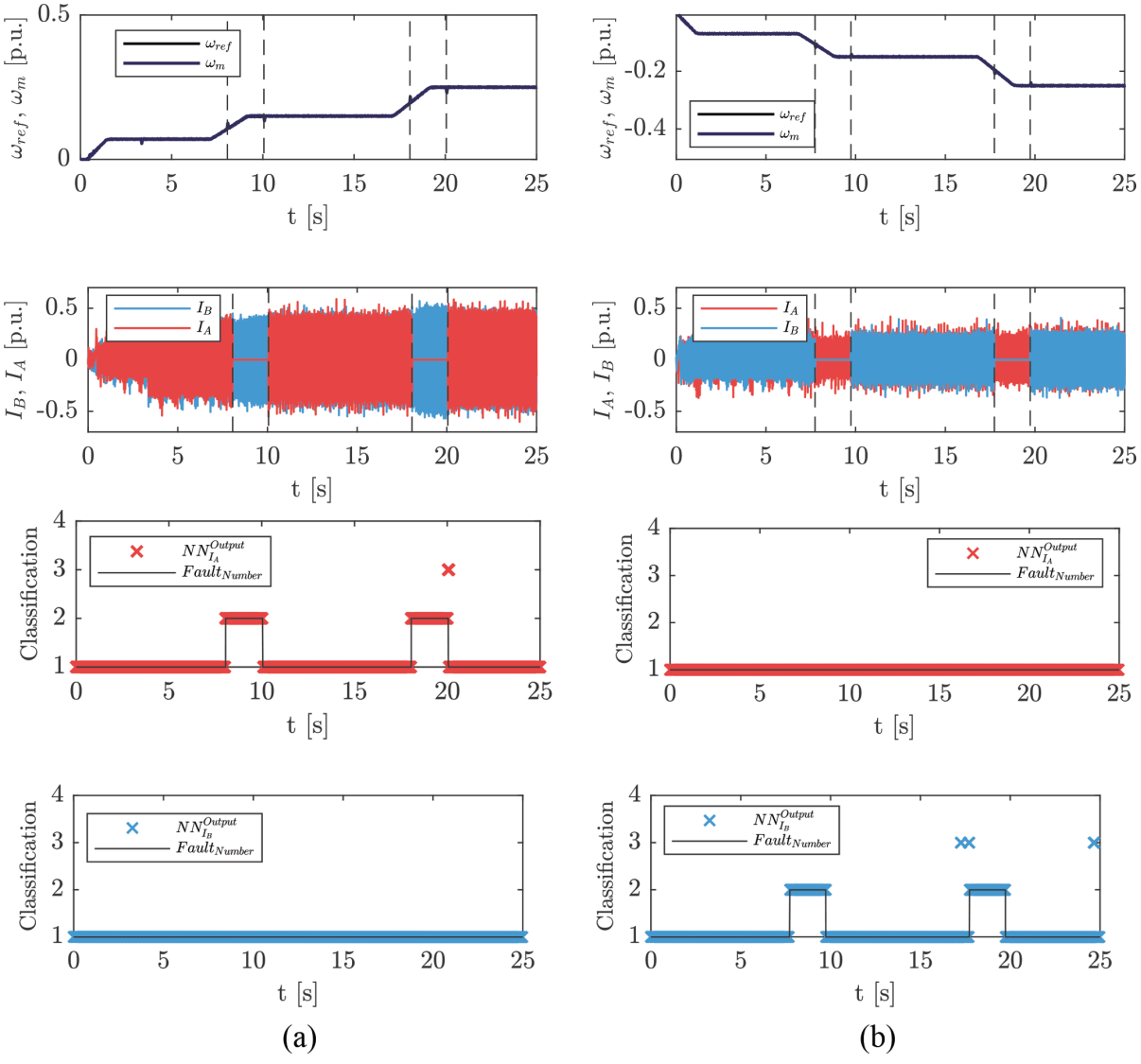

Figure 14. Speed, current, and classifier outputs transients during signal loss and load condition in phase A (a) and non-load condition in phase B (b).

The final example presents the most challenging case to detect, namely measurement noise and gain error in the system operating in regenerative mode (Fig. 15). The presented waveforms demonstrate high classification effectiveness even under these conditions.

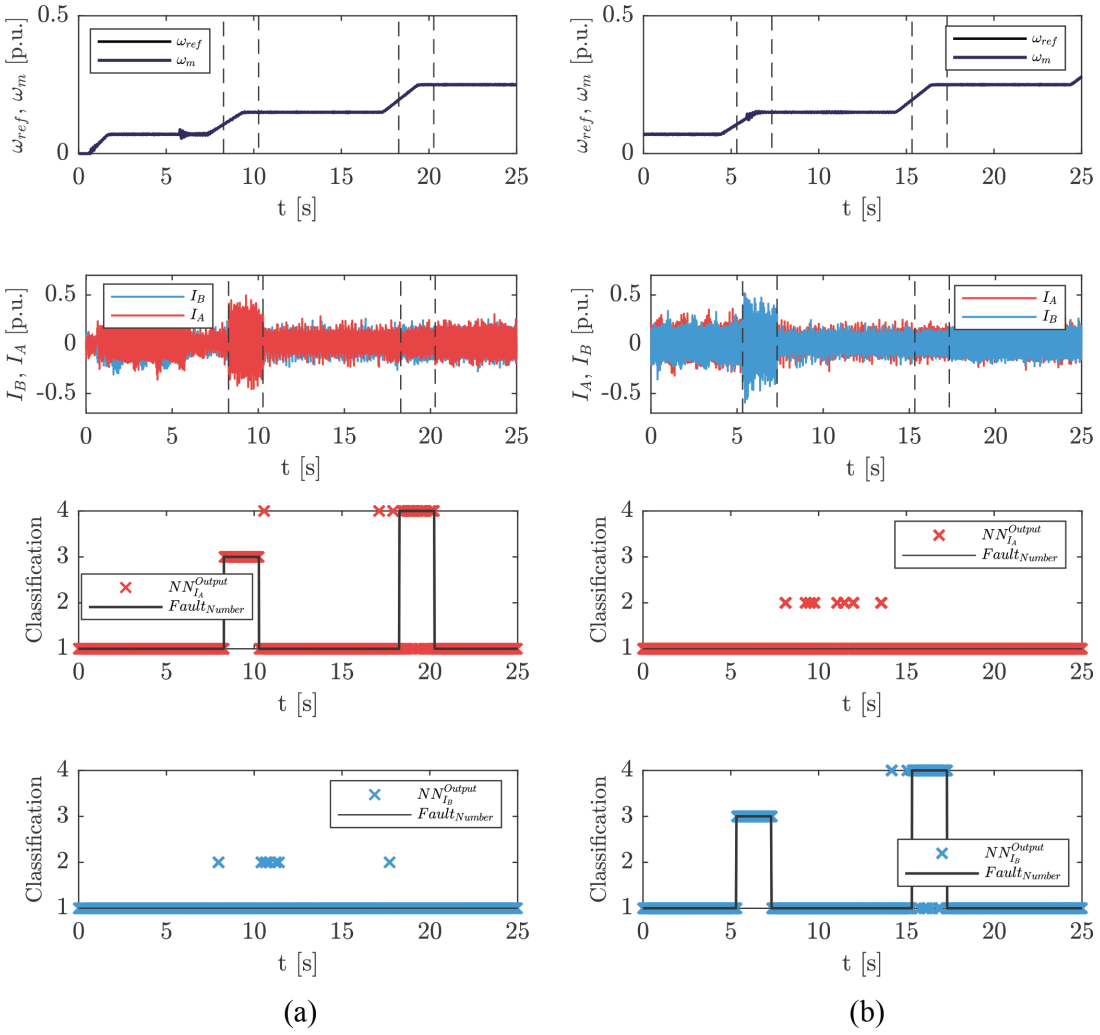

Figure 15. Speed, current, and classifier outputs transients during signal noise and gain error in regenerative mode conditions in phases A (a) and B (b).

6. Conclusion

This paper presents the possibilities of detection and classification of current-sensor faults in a PMSM drive system. The developed fault detection and localisation system is characterised by low computational complexity and moderate effectiveness – slightly above 80%. The classifier based on shallow neural networks offers relatively high accuracy and simple hardware implementation. When analysing individual fault types, only for the gain error, does the effectiveness not exceed 90%. The highest performance, however, was achieved with the classifier based on a CNN, which involves a higher degree of system complexity (4 million operations for the analysis of a single input, which translates into an execution time on a microprocessor at the level of several milliseconds). The use of CNN allows the classifier to achieve correct responses for most fault types at a level of approximately 99%.

When analysing the practical applicability of the studied detection systems, it is important to first consider the imposed requirements. Each of the systems can be implemented on an industrial microprocessor. The execution time for processing a single input varies: it ranges from fractions of a microsecond for detectors based on Cri markers to several tens of milliseconds for classifiers based on CNNs. Another important factor is the input complexity of the system. For marker-based and shallow neural network methods, the complexity is low, whereas due to the size and nature of the matrices in CNNs, it can be considered medium. In summary, when immediate

online fault diagnosis is required without detailed information about the type of fault, Cri markers are the most suitable choice. In contrast, neural network–based systems, particularly convolutional networks, are better suited for applications where diagnosis does not need to be instantaneous and additional information about the fault is available, which can support and optimise maintenance operations.

Acknowledgements

This work was supported by the National Science Centre Poland under project 2024/53/N/ST7/01579.

References

Baharvand, A. H., Fard, S. H. B., Poursaeed, A. H. and Doostizadeh, M. (2024). A novel optimized CNN-SVM approach for inter-turn stator fault detection and localization in permanent magnet synchronous motors. In: *2024 7th International Conference on Electric Power and Energy Conversion Systems (EPECS)*, Sharjah, United Arab Emirates. pp. 1–6. doi: 10.1109/EPECS62845.2024.11006765

Bahri, I., Naouar, M., Slama-Belkhodja, I. and Monmasson, E. (2007). FPGA-based FDI of faulty current sensor in current controlled PWM converters. In: *Proceedings of the EUROCON 2007—The International Conference on Computer as a Tool*, Warsaw, Poland. pp. 1679–1686.

Bishop, M. C. (1996). *Neural Networks for Pattern Recognition*. New York: Oxford University Press.

Chen, B., Yang, J., Li, H., Yang, L. and Zhao, H. (2025). Fault Detection and Identification of PMSM Current Sensor Based on Attention Mechanism and Bidirectional Long Short-Term Memory Network. *IEEE Journal of Emerging and Selected Topics in Power Electronics*, 13(5), pp. 6494–6506. doi: 10.1109/JESTPE.2025.3568200

Guo, C., Wu, C. and Liu, H. (2021). A Sign Logic-Based Method of Current Sensor Fault Detection for PMSM Drivers. *Journal of Sensors*, p. 9955348. doi: 10.1155/2021/9955348

Haghgooei, P., Chaithongsuk, S., Jamshidpour, E., Baghli, L. and Takorabet, N. (2023). Current Sensor Fault Tolerant Strategy for a Wound Rotor Synchronous Machine. In: *ITEC Asia-Pacific 2023*, Chiang Mai, 1–7. doi:10.1109/ITECAsia-Pacific59272.2023.10372228.

Jankowska, K. and Dybkowski, M. (2022). Experimental Analysis of the Current Sensor Fault Detection Mechanism Based on Cri Markers in the PMSM Drive System. *Applied Sciences*, 12, p. 9405. doi: 10.3390/app12199405

Jankowska, K. and Dybkowski, M. (2023). Experimental Analysis of the Current Sensor Fault Detection Mechanism Based on Neural Networks in the PMSM Drive System. *Electronics*, 12, p. 1170. doi: 10.3390/electronics12051170

Jankowska, K., Petro, V., Dybkowski, M. and Kyslan, K. (2023). The Application of a Sliding Mode Observer in a Speed Sensor Fault Tolerant PMSM Drive System. *IEEE Access*, 11, pp. 130899–130908. doi: 10.1109/ACCESS.2023.3335121

Jawdeh, S. A., Li, P. and Bazzi, A. M. (2025). A hybrid fault detection and identification method for current sensor faults in PMSM drives. In: *SDEMPED 2025*, Dallas, 1–6. doi: 10.1109/SDEMPED53223.2025.11154291.

Khil, S. K. E., Jlassi, I., Estima, J. O., Mrabet-Bellaaj, N. and Cardoso, A. J. M. (2017). Detection and isolation of open-switch and current sensor faults in PMSM drives through stator current analysis. In: *SDEMPED 2017*, Tinos, pp. 373–379. doi: 10.1109/DEMPED.2017.8062382.

Khojet El Khil, S., Jlassi, I., Cardoso, A. J. M., Estima, J. O. and Mrabet-Bellaaj, N. (2019). Diagnosis of open-switch and current sensor faults in PMSM drives through stator current analysis. *IEEE Transactions on Industry Applications*, 55(6), pp. 5925–5937. doi: 10.1109/TIA.2019.2930592.

Klimkowski, K. and Dybkowski, M. (2015). Adaptive fault tolerant direct torque control structure of the induction motor drive. In: *EDPE 2015*, Tatranska Lomnica, pp. 7–12.

Li, F., Zhang, B. S., Wang, K., Liu, J. H., Guo, L. L., Liu, Z. Q., Nie, J. and Ge, H. J. (2025). Fault Diagnosis of Current Sensors for Dual Three-Phase PM Machines Based on Harmonic Current. *IEEE Transactions on Industry Applications*, 61(6), pp. 9316–9325. doi: 10.1109/TIA.2025.3571827

Li, H., Qian, Y., Asgarpoor, S. and Sharif, H. (2019). A sensor fault isolation scheme for co-existence of PMSM current sensor and non-sensor imbalance faults. In: *APEC 2019*, Anaheim, pp. 2608–2613. doi: 10.1109/APEC.2019.8722075.

Li, H., Zhu, Z.-Q., Azar, Z., Clark, R. and Wu, Z. (2025). Fault Detection of Permanent Magnet Synchronous Machines: An Overview. *Energies*, 18(3), p. 534. doi: 10.3390/en18030534

Li, Z., Wu, Q., Yang, S. and Chen, X. (2022). Diagnosis of Rotor Demagnetization and Eccentricity Faults for IPMSM Based On Deep CNN and Image Recognition. *Complex Intell Syst*, 8, pp. 5469–5488. doi: 10.1007/s40747-022-00764-z

Ma, K., Wu, S., Kong, D. and Wang, X. (2025). Rolling Bearing Fault Diagnosis Based on VMD-CNN-SLSTM Model. In: *ICMA 2025*, Beijing, pp. 78–84. doi: 10.1109/ICMA65362.2025.11120800.

Nesri, M., Benkadi, H., Nounou, K., Sifelislam, G. and Benkhoris, M. F. (2024). Fault Tolerant Control of a Dual Star Induction Machine Drive System using Hybrid Fractional Controller. *Power Electronics and Drives*, 9(1), pp. 161–175. doi: 10.2478/pead-2024-0010

Sergakis, A., Salinas, M., Gkiolekas, N. and Gyftakis, K. N. (2025). A Review of Condition Monitoring of Permanent Magnet Synchronous Machines: Techniques, Challenges and Future Directions. *Energies*, 18(5), p. 1177. doi: 10.3390/en18051177

Skowron, M., Orlowska-Kowalska, T. and Kowalski, C. T. (2022). Detection of Permanent Magnet Damage of PMSM Drive Based on Direct Analysis of the Stator Phase Currents Using Convolutional Neural Network. *IEEE Transactions on Industrial Electronics*, 69(12), pp. 13665–13675. doi: 10.1109/TIE.2022.3146557

Tarkhani, R., Krim, S., Mansouri, M. and Faouzi Mimouni, M. (2025). Robust Current Sensor Fault-Tolerant Controller Using Third Order Super-Twisting Sliding Mode Observer and Controller for Induction Motors. *IEEE Access*, 13, pp. 52841–52862. doi: 10.1109/ACCESS.2025.3553367

Teler, K., Skowron, M. and Orlowska-Kowalska, T. (2024). Fault Classification of Stator Current Sensors using LSTM Neural Network in an Induction Motor Drive. In: *PEMC 2024*, Pilsen, pp. 1–6. doi:10.1109/PEMC61721.2024.10726366.

Teler, K., Skowron, M. and Orlowska-Kowalska, T. (2024). Implementation of MLP-Based Classifier of Current Sensor Faults in Vector-Controlled Induction Motor Drive. *IEEE Transactions on Industrial Informatics*, 20(4), pp. 5702–5713. doi: 10.1109/TII.2023.3336348

Wang, S., Yang, Z. and Zhang, Q. (2025). A Neural Network-Based Fault-Tolerant Control Method for Current Sensor Failures in Permanent Magnet Synchronous Motors for Electric Aircraft. *Aerospace*, 12(8), p. 697. doi: 10.3390/aerospace12080697

Wu, S., Ma, G., Yao, C., Sun, Z. and Xu, S. (2024). Current Sensor Fault Detection and Identification for PMSM Drives Using Multichannel Global Maximum Pooling CNN. *IEEE Transactions on Power Electronics*, 39(8), pp. 10311–10325. doi: 10.1109/TPEL.2024.3395290

Xiaobing, N. and Shangbo, L. (2022). Research on fault diagnosis and fault tolerant control of PMSM current sensor. In: *CIEEC 2022*, Nanjing, pp. 969–975. doi: 10.1109/CIEEC54735.2022.9846692.

Xu, Y., Feng, K., Xu, S., Chen, X., Yang, W., Liu, F. and Chai, Y. (2024). Current Sensor Incipient Fault Diagnosis in PMSM Drive Systems Using Novel Interval Sliding Mode Observer. *IEEE Transactions on Instrumentation and Measurement*, 73, pp. 1–11. doi: 10.1109/TIM.2024.3351232

Yan, X. and Sun, B. (2023). A multi-dilated fusion convolutional neural network for fault diagnosis of rolling bearings. In: *CPEEE* 2023, Tokyo, pp. 322–325. doi: 10.1109/CPEEE56777.2023.10217584.

Zhang, G., Wang, G., Wang, G., Huo, J., Zhu, L. and Xu, D. (2018). Fault diagnosis method of current sensor for PMSM drives. In: *IPEC-Niigata 2018 – ECCE Asia*, Niigata, pp. 1206–1211. doi: 10.23919/IPEC.2018.8507811.

Zhang, W., Lian, C., Wang, H. and Xu, G. (2025). Research on current sensor fault diagnosis strategy for PMSM drive systems. In: *ISSMAS 2025*, Zhuhai, pp. 48–52. doi: 10.1109/ISSMAS65783.2025.11102807.

Zhao, K., Li, P., Zhang, C., Li, X., He, J. and Lin, Y. (2017). Sliding Mode Observer-Based Current Sensor Fault Reconstruction and Unknown Load Disturbance Estimation for PMSM Driven System. *Sensors*, 17(12), p. 2833. doi: 10.3390/s17122833

Zhao, W., Chen, Y., Tao, T., Ding, S. and Zhang, T. (2025). Open-Phase Fault and Current Sensor Fault Diagnosis Based on Spatial Distributions of Phase Currents for Dual Three-Phase PMSM Drives. *IEEE Transactions on Industrial Electronics*, 72(5), pp. 4375–4388. doi: 10.1109/TIE.2024.3476965

Zheng, X., Zhang, X., Liu, X. and Yuan, X. (2025). A New Signal-Based Diagnosis Method for Current Sensor and Open-Circuited Faults of a Nine-Phase Open-End Winding PMSM. *IEEE Transactions on*

Transportation Electrification, 11(1), pp. 1214–1222. doi: 10.1109/TTE.2024.3402245

Zhu, Z., Shi, T., Lin, Z., Li, C., Chen, H. (2024). An improved fault-tolerant control for PMSM with current sensor fault. In: *2024 27th International Conference on Electrical Machines and Systems (ICEMS)*, Fukuoka, Japan, pp. 2281–2286. doi: 10.23919/ICEMS60997.2024.10921397.